NRC·CNRC

NRC Publications Archive
Archives des publications du CNRC

Compressive creep deformation of lithium foil at varied cell conditions

Ding, Shaochen; Fairgrieve-Park, Logan; Sendetskyi, Oles; Fleischauer, Michael D.

This publication could be one of several versions: author's original, accepted manuscript or the publisher's version. / La version de cette publication peut être l'une des suivantes : la version prépublication de l'auteur, la version acceptée du manuscrit ou la version de l'éditeur.
For the publisher's version, please access the DOI link below./ Pour consulter la version de l'éditeur, utilisez le lien DOI ci-dessous.

Publisher's version / Version de l'éditeur:
https://doi.org/10.1016/j.jpowsour.2020.229404
Journal of Power Sources, 488, 2021-01-15

NRC Publications Archive Record / Notice des Archives des publications du CNRC :
https://nrc-publications.canada.ca/eng/view/object/?id=c11a6363-f471-461e-b779-9a102ccf3d12
https://publications-cnrc.canada.ca/fra/voir/objet/?id=c11a6363-f471-461e-b779-9a102ccf3d12

Access and use of this website and the material on it are subject to the Terms and Conditions set forth at
https://nrc-publications.canada.ca/eng/copyright
READ THESE TERMS AND CONDITIONS CAREFULLY BEFORE USING THIS WEBSITE.

L'accès à ce site Web et l'utilisation de son contenu sont assujettis aux conditions présentées dans le site
https://publications-cnrc.canada.ca/fra/droits
LISEZ CES CONDITIONS ATTENTIVEMENT AVANT D'UTILISER CE SITE WEB.

Questions? Contact the NRC Publications Archive team at PublicationsArchive-ArchivesPublications@nrc-cnrc.gc.ca. If you wish to email the authors directly, please see the first page of the publication for their contact information.

Vous avez des questions? Nous pouvons vous aider. Pour communiquer directement avec un auteur, consultez la première page de la revue dans laquelle son article a été publié afin de trouver ses coordonnées. Si vous n'arrivez pas à les repérer, communiquez avec nous à PublicationsArchive-ArchivesPublications@nrc-cnrc.gc.ca.

National Research Council Canada | Conseil national de recherches Canada

Canada

Compressive creep deformation of lithium foil at varied cell conditions

Shaochen Ding[a], Logan Fairgrieve-Park[b,1], Oles Sendetskyi[b], Michael D. Fleischauer[a,b,*]

[a] *National Research Council - Nanotechnology Research Centre, 11421 Saskatchewan Dr., Edmonton AB T6G 2M9 Canada*
[b] *Department of Physics, University of Alberta, Edmonton AB T6G 2E1 Canada*

[*] Corresponding author
Email address: michael.fleischauer@nrc.ca (Michael D. Fleischauer)
[1] now at Department of Physics, McGill University, Montréal, QC H3A 2T8 Canada

Abstract

Lithium metal rechargeable batteries have great potential for higher energy density storage systems. Current configurations of all solid-state and anode-free cells depend on significant internal mechanical pressure (typically 0.5 - 1 MPa) to reduce interfacial resistance and suppress lithium dendrite formation. Mechanical stack pressure can increase over time and with use as cell components degrade. Lithium is soft at room temperature and may not be physically strong enough to support the required stack pressures in standard lithium-ion operating conditions. Compressive creep deformation of low aspect ratio lithium metal foils was measured in hermetically sealed, rigid but flexible cells at temperatures between 30 - 60°C and applied pressures between 0.6 - 3.6 MPa. Creep rates were typically on the order of a few μm h^{-1}, depending on pressure, temperature, lithium thickness, and grain size. While difficult to notice during fast cycling these creep rates could have a pronounced effect during storage or practical use. Results suggest that pure lithium may not be strong enough for use in high energy density all solid-state devices, and that alternatives (e.g. lithium-rich alloys) should be considered.

Keywords: Creep deformation, lithium, solid-state batteries, anode-free batteries

1. Introduction

Lithium-ion batteries dominate the market for portable, rechargeable energy storage due to their high power and energy density, long cycle life, and low capital costs.[1, 2, 3] Lithium metal is receiving significant research attention as a potential next generation negative electrode material because it can offer a $\sim$ 50% increase in cell energy density compared to conventional graphite.[4, 5] There are, however, a number of challenges associated with lithium metal electrodes due to its mechanical and chemical properties, leading to low coulombic efficiencies, short cycle life, and safety issues in all solid-state and anode-free

cells.[6, 7] For example, stripping lithium at high current densities can lead to void formation in the electrodes.[8] Subsequent plating then results in dendrite formation and growth during cycling, which will deplete lithium and even penetrate through the electrolyte, causing cell failure.[8, 9, 10]

Routes to inhibiting dendrite formation include textured current collectors,[11] protective layers,[12, 13] additives to liquid electrolytes,[14] and applied mechanical pressure.[15, 16] Mechanically stiff solid state electrolytes were theorized to be effective at preventing dendrite propagation.[17] Recent work has demonstrated that (soft) lithium can penetrate through stiff polymer and nearly defect-free crystalline electrolytes.[18, 19, 20] Applied mechanical stack pressure is necessary to not only ensure proper contact at the lithium - electrolyte interface,[21, 22, 23] but also to suppress void formation through beneficial creep.[8, 24, 25, 26] While beneficial creep is important, detrimental creep could, in extreme cases (which we show here are actually standard conditions), lead to lithium extrusion around the electrolyte and separator, and shorting of the cell.

Creep deformation is highly dependent on homologous temperature and pressure. Lithium metal has a relatively low melting point (181°C) / high homologous temperature which should result in substantial lithium creep deformation near room temperature.[27, 28, 29] Commercial Li-ion cells are now required to withstand use and storage at temperatures approaching 60°C. Other niche applications, such as medical devices, must be able to withstand 120°C; many other high value applications require even higher temperatures.[30]

LePage *et al.* investigated tensile creep behaviour of lithium foil cut outs.[31] They concluded that creep by dislocation glide has a power law relationship with pressure and temperature. Masias *et al.* quantified the compressive and tensile creep behaviour of bulk samples of lithium and found similar results to that of LePage.[32] Masias *et al.* used lithium rods with a diameter of 12.7 mm, and aspect ratios (thickness:width) of 4:1 to 1:1 for compressive creep under a variety of pressures. Li foil used in research cells is typically less than 1 mm thick with an aspect ratio of < 0.1:1. Much thinner layers of lithium are utilized in commercial cells, where 0.03 mm thick electroplated Li (aspect ratio < 0.001:1) is treated as

optimal for anode-free cell designs.[5, 14] Masias *et al.* identified aspect ratio, which led to barreling, as a problem affecting surface area measurement and thereby pressure determination. Aspect ratio may also affect yield strength - bulk lithium yields at 0.4 - 1.2 MPa at ambient temperature,[33, 34, 35] whereas micron-scale lithium pillars exhibited yield strength of up to 100 MPa.[36] Data on the length scales of tens to hundreds of microns relevant for research and commercial grade lithium metal cells is scarce.[35, 37]

Stack pressures required to ensure low resistance, stable electrode / electrolyte interfaces for standard Li-ion cells are 0.4 - 1 MPa.[19, 21, 38] Cell stack pressure can also increase over time with electrode and electrolyte breakdown (e.g. from 0.8 to 1.2 MPa).[39] However, many studies use cell stack pressures of $\sim$10 [8, 40, 41] or many 10s of MPa.[22, 24, 42] Thus, more insight is needed into the relevant operation pressure range of lithium-metal based batteries.

To the best of our knowledge the compressive creep behaviour of lithium metal foils has not been reported and could differ substantially from that of bulk lithium. Here, we report on the compressive creep of lithium foil at commercially-relevant pressures and temperatures using a compressible but rigid and fully sealed electrochemical cell, a mechanical force-displacement test system, and optical windows for dynamic surface area and pressure measurement. We found significant creep deformation rates that are highly dependent on lithium aspect ratio, applied pressure, and temperature. The results presented here suggest that special engineering solutions might be needed to prevent detrimental creep in all solid-state and alkali-metal batteries.

2. Experimental

Creep testing was performed by integrating a Conflat-style electrochemical cell[43, 44] featuring welded bellows and an optical window with an Instron 5966 Universal Testing System (which measures / controls force and displacement, and temperature). Creep rates were determined using time-dependent displacement data after reaching a constant applied force. Although creep is in general a three dimensional process, creep rates reported here only describe uniaxial

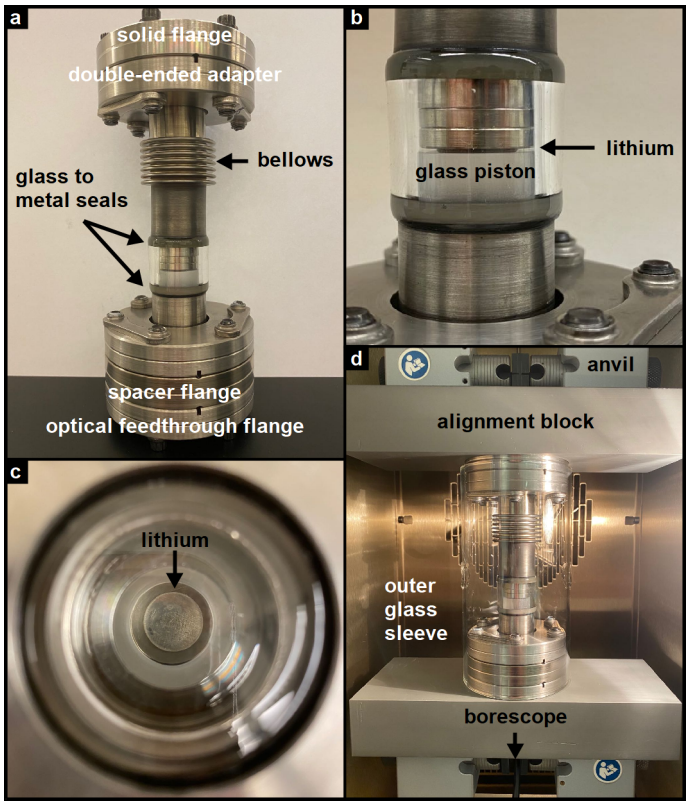

Figure 1: a) Conflat-style cell with welded bellows that remains sealed while allowing for vertical displacement. Individual flanges and the adapter are indicated. b) Side view of 0.33 mm thick lithium foil within a cell. c) End view of lithium within a cell (through a glass piston, glass disk, and an optical viewport. d) Aligned bellows cell within the Instron temperature control chamber. Components are indicated and described in the text.

strain parallel to the applied force. Applied forces were converted to pressures by repeated imaging of the lithium surface area with a borescope. Details are provided below.

2.1. Cell components and assembly

Conflat-style flanges produce ultra-high vacuum tight seals by impinging knife edges into more compliant materials (e.g. copper gaskets). Here this enabled the study of lithium creep without any atmospheric reactions. Glass-to-metal adapters enable electrical isolation of the flanges and bellows permit compression of up to a few mm with minimal force and without compromising

adapter integrity. Double-ended glass-to-metal Conflat adapters with welded bellows (Larson Electronic Glass, Redwood City, CA USA) were used as the key structure of the assembled cell shown in Fig. 1a). Standard Conflat cell assembly using solid steel flanges is described elsewhere.[44] Here, the bottom Conflat flange was replaced with a Conflat double-ended adapter (purchased from AN-Corp, Willston, FL USA) and a Conflat glass viewport (Larson) for the purpose of plan-view image capture. Internal components below the test sample were replaced with a polished glass rod with frosted sides (JT OPTEC, Changchun, Jilin China) directly beneath the lithium, and a glass disk (McMaster-Carr, Los Angeles, CA USA) to transmit force from the rod to the steel rim of the Conflat glass viewport. Each end of the glass piston was used only once to prevent changes in surface roughness from influencing deformation rates. Internal stainless steel and glass alignment sleeves were used to ensure the top steel and lower glass pistons were concentric within 0.5 mm. Piston alignment and the position of the lithium foil are shown in Fig. 1b). A view of lithium foil incorporated within the cell (through the glass rod, disk, and viewport) is provided as Fig. 1c).

Test cells were assembled upright in an Ar-filled glove box maintained at <5 ppm H_2O and O_2, as described previously.[44] Prior to cell assembly, all internal components were cleaned by rinsing with acetone and baked at 80°C for 10 hours before being brought into the glove box. 13 mm Li disks were punched from 2.5, 1.0, or 0.33 mm thick battery-grade lithium foil (Albemarle, Kings Mountain, NC USA), unless otherwise indicated. The lithium foil was lightly brushed prior to cell assembly. The total height of the internal component stack was adjusted by swapping out steel disks such that there would be a small gap between the flanges and stack when the cell was tightened together during the assembly process. This process ensured that no unwanted initial compressive force was applied to the stack before testing. During testing, the bellows were compressed by applying force to the flanges which make contact with the stack and compress the lithium. Custom-made outer alignment sleeves were used during and after cell assembly to ensure alignment of the top and bottom flanges during cell

transport (from the glovebox to Instron test system) and testing. The outer glass alignment sleeve shown in Fig. 1d) also has holes for electrical connections and to improve airflow around the test cell within the Instron temperature control chamber.

2.2. Mechanical and optical measurements

Creep testing was performed by integrating the Conflat-style cell with an Instron 5966 Universal Testing System with a temperature control chamber (Instron model 3119-600) as shown in Fig. 1d). Instron software was used to control the applied forces of up to 500 N along the axis of the Conflat cell and measure the resulting displacement. Force resolution, based on published specifications of our 10 kN load cell, is ±0.5 % down to 10 N. Applied forces varied by less than ±1 N during the force holds. Day-to-day repeatability is on the order of 5 N between 20 and 500 N. Displacement resolution is 0.025 mm with a noise of ±0.0015 mm. Forces were transmitted from the Instron anvils to the Conflat cell using custom-machined anodized aluminum alignment blocks. Force-displacement curves were collected on complete cells (without lithium) at 500 N at 50°C for 24 hours to verify that all creep can be attributed to the lithium under test.

Test chamber temperature was programmed using a Eurotherm 3208 Controller and verified using a resistance temperature detector. Nominal and actual temperatures matched within 1°C; temperature stability was ±0.5°C.

Each test started with all components and instruments at room temperature. After incorporation within the anvils and temperature control chamber the Instron extension and force were zeroed, and data collection started. Displacement data was collected every 10 s. An initial force of 20 N was applied for the first 2 h while the test chamber was brought to the desired temperature at a rate of 1°C min^{-1}. Thermal expansion of the entire test apparatus was approximately 7 μm $^{\circ}\text{C}^{-1}$. After holding at 20 N, the forces were increased to each of 200 N, 300 N, 400 N, 500 N (to target 1 - 4 MPa) with 20 N min^{-1} ramps between forces, and 20 hour holds at each force setpoint. One sample

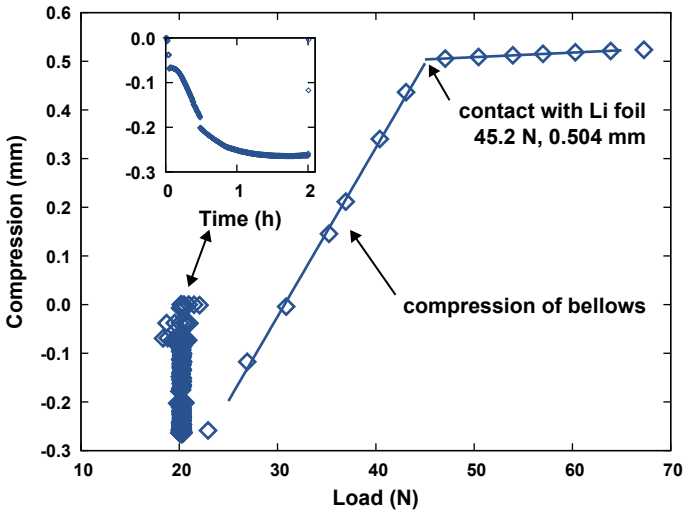

Figure 2: Compression vs. load data during the temperature equilibration (in this case at 40°C) and initial contact between the pistons and Li foil. Compression vs. time data during the temperature equilibration is provided in the inset. Linear fits to the compression vs. load data before and after contact are shown.

(indicated below) was cut to a diameter of 8 mm and held at forces of 100 N, 140 N, 180 N and 220 N to achieve similar pressures.

Cells were assembled such that there would be no compression of the lithium prior to testing on the Instron system. Initial contact data is presented in Fig. 2. Three regions are apparent - thermal equilibrium during the first two hours, compression of the cell bellows prior to contact with the lithium, and compression of the overall system. The bellows have a spring constant of approximately 40 N mm^{-1}. All pressure and displacement measurements are relative to the contact force and displacement of each sample as in Fig. 2. Additional pressure corrections to account for significant compression of the bellows were included where appropriate. Any following descriptions of force are nominal and used for the sake of clarity.

A Depstech NTC86T 5.0 MP borescope was mounted directly under the cell through a hole in the bottom alignment block. The lithium-to-lens working distance was approximately 3 cm. Images were acquired every 10 min during the approximately 84 h tests. Lithium areas were estimated from the borescope

images by manually comparing the area of the 18.5 mm dia. steel piston to the area of the lithium foil. Area uncertainty is on the order of a few percent.

2.3. Grain size and texture determination

X-ray diffraction patterns were collected on as-supplied, annealed, and annealed and compressed lithium foils using a Bruker D8 diffractometer equipped with a copper micro source and a Vantec 500 area detector. Samples were transferred to the diffractometer using an encapsulation method described elsewhere.[45] Grain sizes for the as-supplied and compressed foils were determined using the γ method,[46] which relies on counting reflections from individual grains on an area detector and comparing the number to the reference sample. A Si NIST 640d standard powder was used as a reference.

Texture measurements were performed on as-supplied foils using the same diffractometer. ϕ scans with a step of 2° at four different ψ angles in the range from 0 to 80° scattering angle were collected, then merged using MAX3D software[47] and individual pole figures for (110), (200) and (211) reflections of lithium were exported. Orientation density function (ODF) plots were calculated from the pole figures using MTEX Matlab toolbox.[48]

3. Results and Discussion

Borescope images of an initially 2.5 mm thick, 13 mm dia. piece of Li foil are provided in Fig. 3. Images are provided immediately prior to contact and after 5, 10, and 20 h at a constant nominal force of 200 N. Dark regions in the center of the lithium are an artifact originating from sample lighting and were observed in all borescope images; lithium extracted from compressed cells maintained its colour but lost some of its lustre. Lithium also roughly retains its circular shape, with some variations at the edge. The corresponding compression-time data is presented in Fig. 4. Plastic deformation and (stage 1) creep are apparent in the first five hours. Steady-state (stage 2) creep occurs after ∼10 h; displacement is nearly linear to 20 h. Creep deformation rates are shown in Fig. 4. Continued creep deformation leads to increasing surface areas; with a constant applied

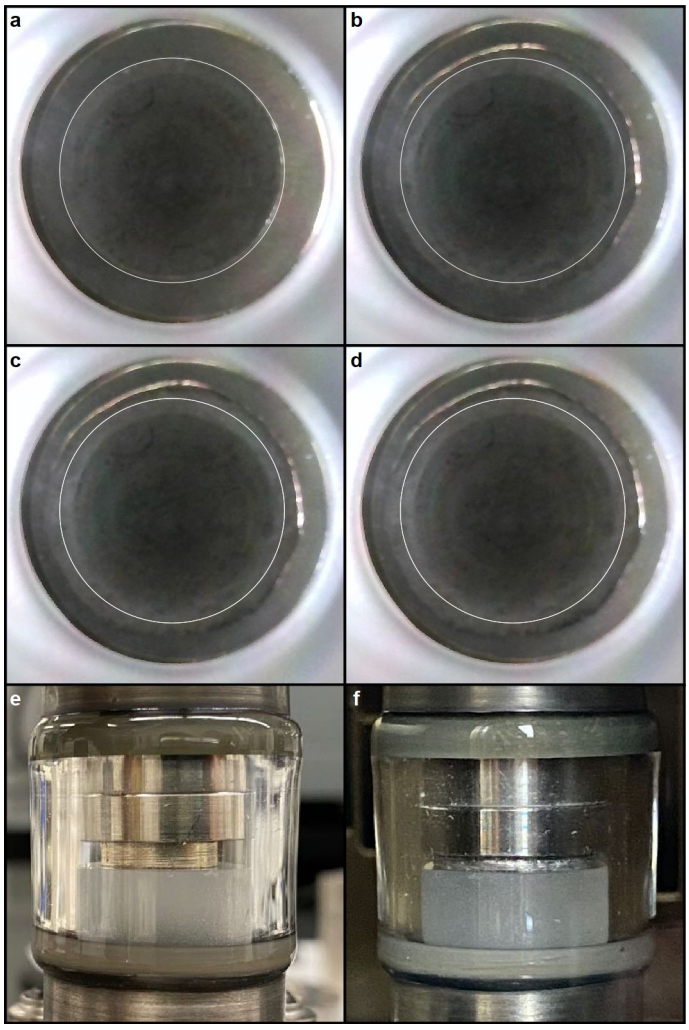

Figure 3: a-d) Borescope images of 2.5 mm thick Li foil after a) 0 b) 5 h c) 10 h and d) 20 h at 30°C and an applied force of 200 N. The initial circumference is superimposed on each image with a white circle. e-f) Side view images of 2.5 mm thick Li e) before compression and f) after 20 h at 200 N and 10 h at 300 N, at 30°C. Photographs were collected while the test cell was in the e) lab and f) temperature control chamber.

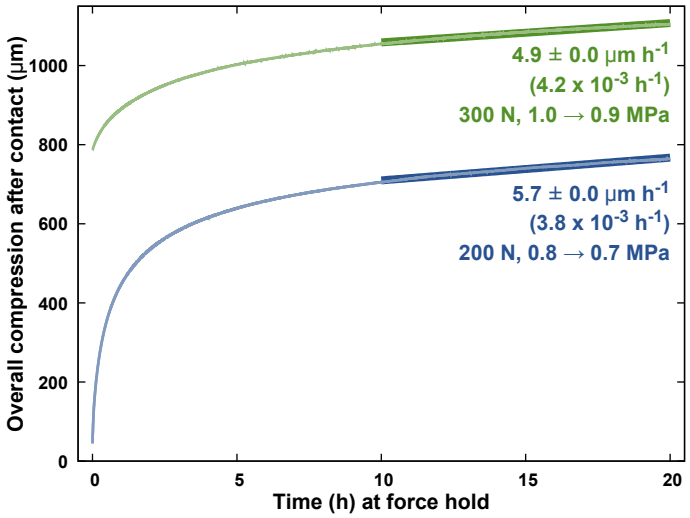

Figure 4: Compression vs. time curves for 2.5 mm thick Li foil. Linear fits to the last 10 hours of data are shown. Creep (and strain) rates, nominal forces, and pressures at the beginning and end of the force hold are indicated.

force of 200 N the applied pressure changes from 0.8 to 0.7 MPa during the last 10 h. Similar trends are observed during a subsequent constant applied force of 300 N.

Creep rates do not reflect the relative change in sample thickness. Strain rates provided in Fig. 4 were calculated by dividing the creep rate by the sample thickness (nominal - compressed) 15 h in to each force hold. Attempts to measure sample thickness with a precision micrometer were unsuccessful as the micrometer clamping pressure caused the lithium to deform. Uncertainty in the initial thickness is specified by the supplier as ±0.01 mm. For both force holds, the strain rate is approximately 4 x 10^{-3} hr^{-1}. This is very substantial. Over the course of a day, such a strain rate would lead to a nearly 10% change in overall electrode thickness, and with moderate manufacturing tolerances, would likely lead to lithium extrusion beyond the current collector and shorting of the cell. Combined plastic and creep deformation reduced the lithium thickness approximately by half and doubled the area after less than two days at moderate pressure (<1 MPa). Side view images of the Li foil prior to compression and 10 h in to the 300 N hold (30 h total in compression) are provided in Fig. 3e and f.

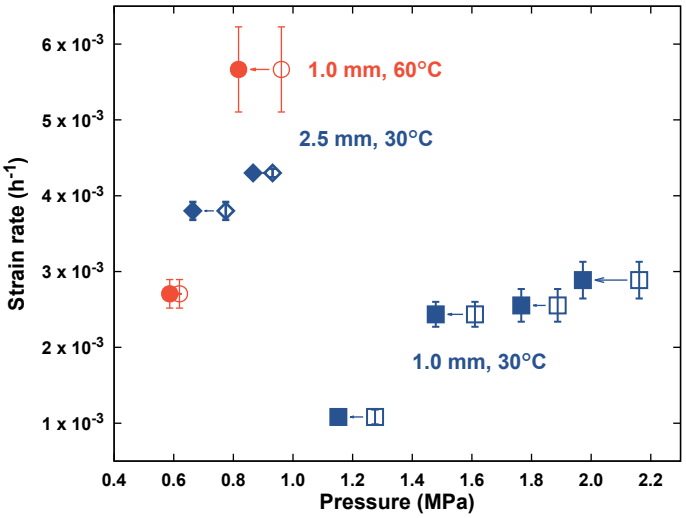

Figure 5: Strain rates as a function of initial lithium thickness, temperature, and pressure. Open and closed symbols represent the pressure after 10 and 20 hours at each force hold, respectively.

Strain rates for 2.5 mm and 1.0 mm initial thickness lithium as a function of pressure are shown in Fig. 5. Data from Fig. 4 is included for the sake of comparison. In all cases the strain rate is substantial and implies a very limited device lifetime at standard temperatures and pressures. Data from four force-holds are provided for the 1.0 mm initial thickness sample tested at 30°C. Only two holds are provided for the 2.5 mm initial thickness sample because the lithium expanded beyond the diameter of the pistons. A 8 mm dia. piece of 1 mm thick foil was tested at 60°C (at lower applied forces, see above) to avoid similar issues. Instead, the borescope, which is only rated for use to 50°C, malfunctioned during the third force hold so area data was not available. A strain rate above 5 x 10^{-3} hr^{-1} at commercially relevant temperatures and pressures is not viable for most applications.

Higher strain rates for thicker samples are in line with previous observations of yield strength (summarized in Fig. 7 of [35]). The question is the relevant length scale - sample thickness or grain size. Creep rates (rather than strain rates, due to the foil thickness being a substantial fraction (1/13) of the Instron displacement resolution) measured on 0.33 mm initial thickness foil are provided

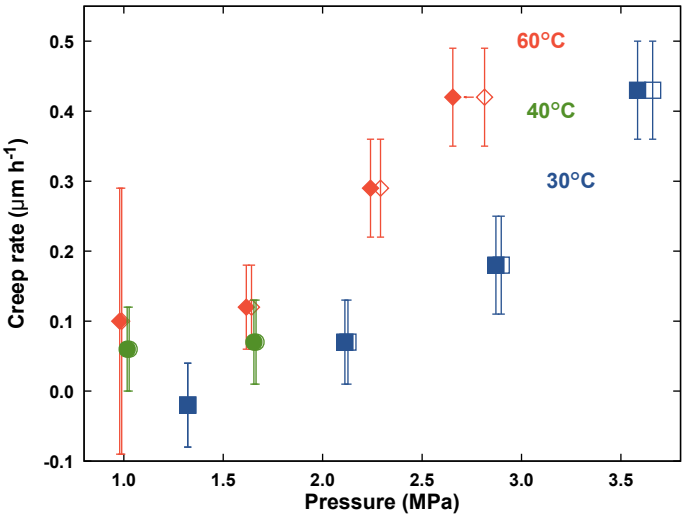

Figure 6: Creep rates as a function of temperature and pressure for 0.33 mm thick Li foil, in the style of Fig. 5. Uncertainty in creep rates from linear fits (as in Fig. 4) is indicated.

in Fig. 6. A creep rate of 0.3 μm hr^{-1} on a 0.3 mm thick sample corresponds to a strain rate of 1 x 10^{-3} hr^{-1}, below all of the strain rates shown in Fig. 5 but higher than desired.

Creep rates at pressures below 1.5 MPa are within uncertainty of zero. Slight changes in temperature have a pronounced effect on creep rates at pressures above 1.5 MPa. Maintaining a cell at pressures below 1.5 MPa is possible but challenges many of the projected routes to high current and energy density devices described above. Data presented in Fig. 6 is not suitable to fit to a multi-parameter power law model but does not appear to have the same substantial pressure dependence as measured by Masias *et al.*[32] and LePage *et al.*[31] LePage noted that frictional forces will have an influence on observed deformation rates. With our very low aspect ratio samples, contact areas and surface areas are effectively the same, and extruded lithium may form a rough interface with the steel and glass surfaces. In addition, lithium contact surfaces were intentionally roughened to remove surface impurities. Optically smooth glass piston ends provide a nominally identical surface roughness but may still contain sub-micron scratches and imperfections. Reusing a glass piston led to

creep suppression until a threshold pressure was applied. Steel pistons were reused for a substantial number of tests (∼20) without noticeable effect.

Microstructure of the Li foil has a strong influence on the strength and plasticity of the foil. The microstructure analysis may offer a more relevant comparison between bulk, foil, and potentially electroplated samples. In particular, we performed grain size analysis of the as-supplied, annealed, and compressed foil using X-ray diffraction. The annealing of the foil will change the grain size and allow us to test the mechanical properties of the Li foil with different microstructure. 0.33 mm thick Li foil was annealed in a glovebox on a calibrated hotplate set to 100°C for 19 hours. The mean grain size of the as-supplied 0.33 mm thick foil was estimated to be 50 μm. Similar measurements on 1.0 mm and 2.5 mm thick lithium suggest grain sizes of 80 and 130 μm, respectively. After annealing of the 0.33 mm thick foil, the grains grew in size with grains as large as 450 μm. As there were only a few large grains illuminated by the X-ray beam in the annealed foil, there was not enough statistics for the γ method, therefore the grain size was estimated by comparing the integrated (110) Li peak intensity of individual grains before and after annealing.

Creep deformation rates for as-supplied and annealed 0.33 mm thick Li foil compressed at 50°C are provided in Fig. 7. As-supplied data collected at 50°C follows the same trend as the 30, 40 and 60°C data presented in Fig. 6. The annealed sample, with much larger grains (similar in size to the overall sample thickness), exhibits similar creep rates at lower pressures and larger creep rates at higher pressure. This can be attributed to unobstructed dislocation movement within large grains in the annealed foil, while smaller grains would obstruct the dislocation movement at the grain boundaries in the as-supplied foil. Interestingly, the mean grain size of the annealed Li foil decreased after compression and creep deformation and was estimated to be 28 μm using the same γ method[46]. This suggests grain size reduction due to compression and creep deformation. Work hardening during rolling of lithium to the specified initial thickness may impart similar changes in grain size and explain some of the thickness dependence of strain rate in otherwise identical conditions. X-ray

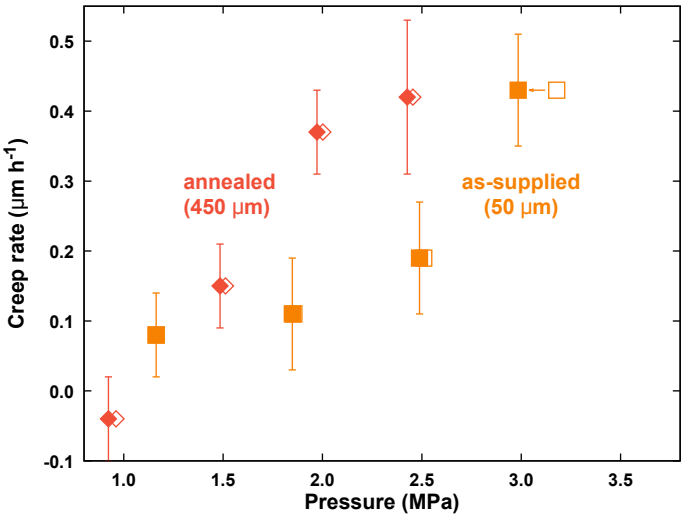

Figure 7: Creep rates as a function of pressure and annealing condition for 0.33 mm thick Li foil measured at 50°C, in the style of Fig. 5. Estimated grain sizes are indicated.

diffraction texture measurements of as-supplied foils show that our thinnest foil of 0.33 mm has a distinct rolling texture with [200] crystallographic direction pointing out of the plane of the foil (along the normal direction), which is consistent with previous reports[49, 50, 51]. We also find a clear preferred orientation in the rolling and transverse direction of the 0.33 mm foil that resembles twinning with rotation of the grains relative to the [200] axis parallel to the normal direction. Orientation density function plots for (110), (200) and (211) reflections are displayed in Fig. 8. The 1 mm thick foil has a similar texture with [200] direction parallel to the normal direction, but much weaker texture in the rolling and transverse direction. This is consistent with the texture reported by LePage *et al.* where there was no observed difference in texture between the rolling direction and transverse direction of the 0.75 mm foil.[31] The 2.5 mm foil has almost no discernible texture. Further studies on the effect of grain size and morphology on creep rates are required.

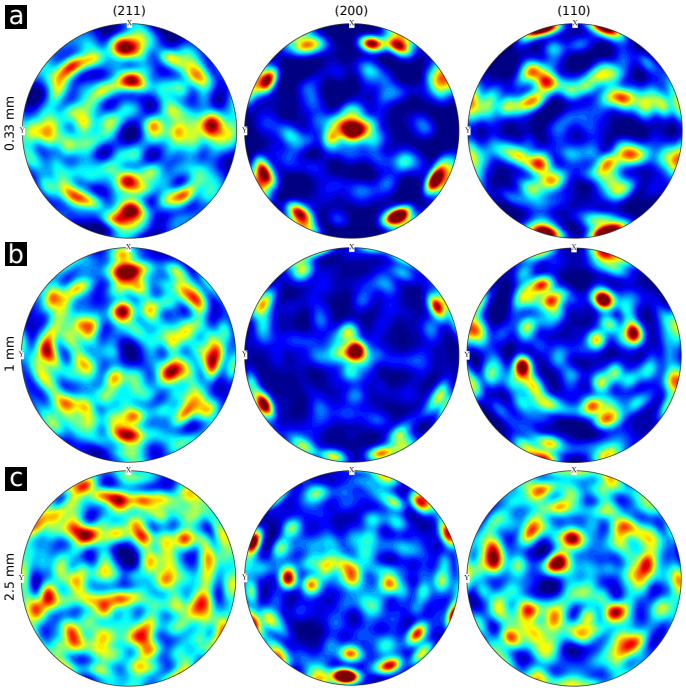

Figure 8: ODF plots for (110), (200) and (211) reflections for a) 0.33 mm, b) 1.0 mm and c) 2.5 mm thick Li foils. X and Y correspond to the rolling direction and transverse direction, respectively.

4. Conclusions

Substantial creep and strain rates were observed in lithium foils compressed at standard, commercially-relevant temperatures and pressures. Deformation rates varied with lithium thickness, temperature, and applied pressure. All samples exhibited significant creep deformation at applied pressures of less than 2 MPa, which suggests that pure Li may not be able to sustain high stack pressures (e.g. > 10 MPa) and alternate approaches to suppress dendrite formation may need to be considered. Although thinner foils and smaller grains exhibit lower deformation rates at a given pressure, it is unclear if this can be sustained in long term device applications without changing the physical properties of the electrode. Possible routes forward may include textured current collectors[11] or lithium-rich alloys with substantially higher melting points / lower homologous temperatures (e.g. β-LiAl, 600°C[52]). Higher resolution displacement studies may allow for direct measurement of the physical properties of very thin (e.g. 0.01 - 0.05 mm) foils and electroplated layers of lithium, as well as the effect of lithium grain size, morphology, and porosity.

Acknowledgements

Funding for this work was provided by Natural Resources Canada - Energy Innovation Program, the National Research Council Canada, and the University of Alberta. The authors thank J.-S. Park, T. Kugler, R. Schwarze, M. Labbe, J. Dibbs, D. Sameoto, and P. Motamedi for helpful suggestions, and B. Olsen for contributions to the graphical abstract. The authors thank B. Yetman and J. Tan (Engineered Power, Calgary AB Canada) for their insight and for providing lithium foil.

References

[1] N. Nitta, F. Wu, J. T. Lee, G. Yushin, Li-ion battery materials: present and future, Materials Today 18 (5) (2015) 252–264. doi:10.1016/j.mattod.2014.10.040.

[2] G. Zubi, R. Dufo-López, M. Carvalho, G. Pasaoglu, The lithium-ion battery: State of the art and future perspectives, Renewable and Sustainable Energy Reviews 89 (2018) 292–308. doi:10.1016/j.rser.2018.03.002.

[3] O. Schmidt, A. Hawkes, A. Gambhir, I. Staffell, The future cost of electrical energy storage based on experience rates, Nature Energy 2 (2017) 17110. doi:10.1038/nenergy.2017.110.

[4] B. D. McCloskey, Attainable gravimetric and volumetric energy density of Li-S and Li ion battery cells with solid separator-protected li metal anodes, The Journal of Physical Chemistry Letters 6 (22) (2015) 4581–4588. doi:10.1021/acs.jpclett.5b01814.

[5] P. Albertus, S. Babinec, S. Litzelman, A. Newman, Status and challenges in enabling the lithium metal electrode for high-energy and low-cost rechargeable batteries, Nature Energy 3 (2018) 16–21. doi:10.1038/s41560-017-0047-2.

[6] K. N. Wood, M. Noked, N. P. Dasgupta, Lithium metal anodes: Toward an improved understanding of coupled morphological, electrochemical, and mechanical behavior, ACS Energy Letters 2 (3) (2017) 664–672. doi:10.1021/acsenergylett.6b00650.

[7] W. Xu, J. Wang, F. Ding, X. Chen, E. Nasybulin, Y. Zhang, J.-G. Zhang, Lithium metal anodes for rechargeable batteries, Energy and Environmental Science 7 (2) (2014) 513–537. doi:10.1039/c3ee40795k.

[8] J. Kasemchainan, S. Zekoll, D. S. Jolly, Z. Ning, G. O. Hartley, J. Marrow, P. G. Bruce, Critical stripping current leads to dendrite formation on plating in lithium anode solid electrolyte cells, Nature Materials 18 (2019) 1105–1111. doi:10.1038/s41563-019-0438-9.

[9] J. Sakamoto, More pressure needed, Nature Energy 4 (2019) 827–828. doi:10.1038/s41560-019-0478-z.

[10] K. N. Wood, E. Kazyak, A. F. Chadwick, K.-H. Chen, J.-G. Zhang, K. Thornton, N. P. Dasgupta, Dendrites and pits: Untangling the complex behavior of lithium metal anodes through operando video microscopy, ACS Central Science 2 (11) (2016) 790–801. doi:10.1021/acscentsci.6b00260.

[11] K. Tantratian, D. Cao, A. Abdelaziz, X. Sun, J. Sheng, A. Natan, L. Chen, H. Zhu, Stable li metal anode enabled by space confinement and uniform curvature through lithiophilic nanotube arrays, Advanced Energy Materials 10 (5) (2019) 1902819. doi:10.1002/aenm.201902819.

[12] W. Li, H. Yao, K. Yan, G. Zheng, Z. Liang, Y.-M. Chiang, Y. Cui, The synergetic effect of lithium polysulfide and lithium nitrate to prevent lithium dendrite growth, Nature Communications 6 (1) (2015) 7436. doi:10.1038/ncomms8436.

[13] A. C. Kozen, C.-F. Lin, O. Zhao, S. B. Lee, G. W. Rubloff, M. Noked, Stabilization of lithium metal anodes by hybrid artificial solid electrolyte interphase, Chemistry of Materials 29 (15) (2017) 6298–6307. doi:10.1021/acs.chemmater.7b01496.

[14] R. Weber, M. Genovese, A. Louli, S. Hames, C. Martin, I. G. Hill, J. Dahn, Long cycle life and dendrite-free lithium morphology in anode-free lithium pouch cells enabled by a dual-salt liquid electrolyte, Nature Energy 4 (8) (2019) 683–689. doi:10.1038/s41560-019-0428-9.

[15] D. Wilkinson, H. Blom, K. Brandt, D. Wainwright, Effects of physical constraints on li cyclability, Journal of Power Sources 36 (4) (1991) 517–527. doi:10.1016/0378-7753(91)80077-b.

[16] T. Hirai, I. Yoshimatsu, J. ichi Yamaki, Influence of electrolyte on lithium cycling efficiency with pressurized electrode stack, Journal of The Electrochemical Society 141 (3) (1994) 611–614. doi:10.1149/1.2054778.

[17] C. Monroe, J. Newman, The impact of elastic deformation on deposition

kinetics at lithium polymer interfaces, Journal of The Electrochemical Society 152 (2) (2005) A396–A404. doi:10.1149/1.1850854.

[18] L. Porz, T. Swamy, B. W. Sheldon, D. Rettenwander, T. Frömling, H. L. Thaman, S. Berendts, R. Uecker, W. C. Carter, Y.-M. Chiang, Mechanism of lithium metal penetration through inorganic solid electrolytes, Advanced Energy Materials 7 (2017) 1701003. doi:10.1002/aenm.20170100.

[19] A. Sharafi, H. M. Meyer, J. Nanda, J. Wolfenstine, J. Sakamoto, Characterizing the Li-$Li_7La_3Zr_2O_{12}$ interface stability and kinetics as a function of temperature and current density, Journal of Power Sources 302 (2016) 135–139.

[20] P. Barai, K. Higa, V. Srinivasan, Lithium dendrite growth mechanisms in polymer electrolytes and prevention strategies, Physical Chemistry Chemical Physics 19 (2017) 20493–20505. doi:10.1039/C7CP03304D.

[21] J. Cannarell, C. B. Arnold, Stress evolution and capacity fade in constrained lithium-ion pouch cells, Journal of Power Sources 245 (2014) 745–751.

[22] J.-M. Doux, H. Nguyen, D. H. S. Tan, A. Banerjee, X. Wang, E. A. Wu, C. Jo, H. Yang, Y. S. Meng, Stack pressure considerations for room-temperature all-solid-state lithium metal batteries, Advanced Energy Materials 10 (1) (2019) 1903253. doi:10.1002/aenm.201903253.

[23] X. Zhang, Q. J. Wang, K. L. Harrison, S. A. Roberts, S. J. Harris, Pressure-driven interface evolution in solid-state lithium metal batteries, Cell Reports Physical Science 1 (2) (2020) 100012. doi:10.1016/j.xcrp.2019.100012.

[24] T. Krauskopf, H. Hartmann, W. G. Zeier, J. Janek, Toward a fundamental understanding of the lithium metal anode in solid-state batteries - an electrochemo-mechanical study on the garnet-type solid electrolyte $Li_{6.25}Al_{0.25}La_3Zr_2O_{12}$, ACS Applied Materials & Interfaces 11 (2019) 14463–14477. doi:10.1021/acsami.9b02537.

[25] M. J. Wang, R. Choudhury, J. Sakamoto, Characterizing the Li-solid-electrolyte interface dynamics as a function of stack pressure and current density, Joule 3 (2019) 2165–2178. doi:10.1016/j.joule.2019.06.017.

[26] X. Zhang, Q. J. Wang, K. L. Harrison, K. Jungjohann, B. L. Boyce, S. A. Roberts, P. M. Attia, S. J. Harris, Rethinking how external pressure can suppress dendrites in lithium metal batteries, Journal of The Electrochemical Society 166 (15) (2019) A3639–A3652. doi:10.1149/2.0701914jes.

[27] P. Sarent, M. Ashby, Deformation mechanism maps for alkali metals, Scripta Metallurgica 18 (2) (1984) 145–150.

[28] H. O. K. Kirchner, Plastic deformation of the alkali metals sodium and potassium., Acta Physica Austriaca 48 (1977) 111–129.

[29] S. Hori, K. Saito, T. Hasegawa, Plastic workability of pure lithium, Journal of Japan Institute of Light Metals 50 (12) (2000) 660–665.

[30] M.-T. F. Rodrigues, G. Babu, H. Gullapalli, K. Kalaga, F. N. Sayed, K. Kato, J. Joyner, P. M. Ajayan, A materials perspective on Li-ion batteries at extreme temperatures, Nature Energy 2 (2017) 17108. doi:10.1038/nenergy.2017.108.

[31] W. S. LePage, Y. Chen, E. Kazyak, K.-H. Chen, A. J. Sanchez, A. Poli, E. M. Arruda, M. Thouless, N. P. Dasgupta, Lithium mechanics: Roles of strain rate and temperature and implications for lithium metal batteries, Journal of The Electrochemical Society 166 (2) (2019) A89–A97. doi:10.1149/2.0221902jes.

[32] A. Masias, N. Felten, R. Garcia-Mendez, J. Wolfenstine, J. Sakamoto, Elastic, plastic, and creep mechanical properties of lithium metal, Journal of Materials Science 54 (2019) 2585–2600. doi:10.1007/s10853-018-2971-3.

[33] M. Wang, J. B. Wolfenstine, J. Sakamoto, Temperature dependent flux balance of the $Li/Li_7La_3Zr_2O_{12}$ interface, Electrochimica Acta 296 (2019) 842–847. doi:10.1016/j.electacta.2018.11.034.

[34] R. Schultz, Lithium: measurement of young's modulus and yield strength, Fermilab Technical Memo 2191 (2002).

[35] C. D. Fincher, D. Ojeda, Y. Zhang, G. M. Pharr, M. Pharr, Mechanical properties of metallic lithium: from nano to bulk scales, Acta Materialia 186 (2020) 215–222. doi:10.1016/j.actamat.2019.12.036.

[36] C. Xu, Z. Ahmad, A. Aryanfar, V. Viswanathan, J. R. Greer, Enhanced strength and temperature dependence of mechanical properties of Li at small scales and its implications for li metal anodes, Proceedings of The National Academy of Sciences 114 (2016) 57–61. doi:10.1073/pnas.1615733114.

[37] Y. Wang, Y.-T. Cheng, A nanoindentation study of the viscoplastic behavior of pure lithium, Scripta Materialia 130 (2017) 191–195. doi:10.1016/j.scriptamat.2016.12.006.

[38] V. Müller, R.-G. Scurtu, M. Memm, M. A. Danzer, M. Wohlfahrt-Mehrens, Study of the influence of mechanical pressure on the performance and aging of lithium-ion battery cells, Journal of Power Sources 440 (2019) 227148. doi:10.1016/j.jpowsour.2019.227148.

[39] A. Louli, M. Genovese, R. Weber, S. Hames, E. Logan, J. Dahn, Exploring the impact of mechanical pressure on the performance of anode-free lithium metal cells, Journal of The Electrochemical Society 166 (2019) A1291–A1299. doi:10.1149/2.0091908jes.

[40] M. Wang, J. Sakamoto, Correlating the interface resistance and surface adhesion of the Li metal-solid electrolyte interface, Journal of Power Sources 377 (2018) 7–11.

[41] T. Krauskopf, B. Mogwitz, C. Rosenbach, W. G. Zeier, J. Janek, Diffusion limitation of lithium metal and Li–Mg alloy anodes on llzo type solid electrolytes as a function of temperature and pressure, Advanced Energy Materials 9 (44) (2019) 1902568.

[42] S. Tariq, K. Ammigan, P. Hurh, R. Schultz, P. Liu, J. Shang, Li material testing-fermilab antiproton source lithium collection lens, in: Proceedings of the 2003 Particle Accelerator Conference, Vol. 3, IEEE, 2003, pp. 1452–1454.

[43] K. Periyapperuma, T. Tran, S. Trussler, D. Ioboni, M. Obrovac, Conflat two and three electrode electrochemical cells, Journal of The Electrochemical Society 161 (2014) A2182–A2187. doi:10.1149/2.0721414jes.

[44] M. D. Fleischauer, M. R. Kupsta, A. D. Johnson, Improved conflat cell for repeatable electrochemical testing to 400°C, Journal of The Electrochemical Society 166 (2019) A398–A402. doi:10.1149/2.0721414jes.

[45] M. Z. Ghavidel, M. R. Kupsta, J. Le, E. Feygin, A. Espitia, M. D. Fleischauer, Electrochemical formation of four al-li phases (β-AlLi, Al_2Li_3, $AlLi_{2-x}$, Al_4Li_9) at intermediate temperatures, Journal of The Electrochemical Society 166 (2019) A4034–A4040. doi:10.1149/2.0061916jes.

[46] B. B. He, Two-dimensional X-ray diffraction, Vol. 2, Wiley Online Library, 2018. doi:10.1002/9781119356080.

[47] J. Britten, W. Guan, R. Sonnadara, Visualization of 3D diffraction: MAX3D update, Foundations of Crystallography 74 (2018) a399.

[48] F. Bachmann, R. Hielscher, H. Schaeben, Texture analysis with MTEX–free and open source software toolbox, in: Solid State Phenomena, Vol. 160, Trans Tech Publ, 2010, pp. 63–68. doi:10.4028/www.scientific.net/SSP.160.63.

[49] F. Shi, A. Pei, A. Vailionis, J. Xie, B. Liu, J. Zhao, Y. Gong, Y. Cui, Strong texturing of lithium metal in batteries, Proceedings of the National Academy of Sciences 114 (46) (2017) 12138–12143. doi:10.1073/pnas.1708224114.

[50] N. Brodusch, K. Zaghib, R. Gauvin, Electron backscatter diffraction applied to lithium sheets prepared by broad ion beam milling, Microscopy Research and Technique 78 (1) (2014) 30–39. doi:10.1002/jemt.22441.

[51] H. Hu, Texture of metals, in: Texture, Vol. 1, Hindawi, 1970.

[52] A. J. McAlister, The Al-Li (Aluminum-Lithum) system, Bulletin of Alloy Phase Diagrams 3 (1982) 177– 183.